LATVIAN JOURNAL OF PHYSICS
AND TECHNICAL SCIENCES
2022, N 6

DOI: 10.2478/lpts-2022-0043

ISOTHERMAL MECHANICAL CYCLING OF SAPONITE–TITANIUM COMPOSITES IN CONDITIONS OF COMPLEX STRESSED STATE

N.M. Huliieva[1,*], V.V. Pasternak[2]

[1] Lutsk National Technical University,
75 Lvivska Str., 43018 Lutsk, UKRAINE
[2] Lesya Ukrainka Volyn National University,
9 Potapova Str., Lutsk 43025, UKRAINE
*e-mail: n.huliieva@lntu.edu.ua

It has been experimentally shown that in the isothermal mechanocycling of continuous cylindrical samples of saponite–titanium composites under conditions of a complex stress state, a reversible deformation of the properties of martensitic inelasticity is observed, which appears during thermal cycling at intervals of martensitic transformations.

According to the results of the experiment, the influence of the ratio between the static and cyclic components of the stress on the change of shear deformation in a complex stress state during mechanical cycling with axial load is estimated.

Keywords: *Complex stress state, cylindrical samples, mechanocycling, orthogonal loading saponite–titanium composites.*

1. INTRODUCTION

Details of executive power mechanisms of different functional purposes in mechanical engineering made materials with the effect of shape memory (ESM) [1]. They are usually under the simultaneous influence of axial and tangential stresses. For their manufacture it is necessary to choose metals or alloys that have the appropriate mechanical characteristics and deformation properties of materials at different temperature and force effects [2]. There are a few publications on the mechanical behaviour of composites based on saponite–titanium and other materials with shape memory in a complex stress state today and this suggests the relevance of the research in this area [3].

ESM, the phenomena of martensitic inelasticity, the effects of multiple reversible shape memory, transformation plasticity, reversible shape memory, deformation of oriented transformation, etc. have been widely studied [4]. The above-mentioned phenomena are usually initiated by martensitic reactions associated with thermal cycling of the material. Work on mechanocycling of ESM material in a complex stress state in most cases is devoted to the determination of long-term strength, less often the structure of the material under similar exposure is studied [5]. The authors [6] recorded that during isothermal mechanocycling in the two-phase state, the material was more plastic and less susceptible to equalization of the voltage intensity amplitude. In [7], it was shown that the active deformation of the ESM material in isothermal conditions may be accompanied by phenomena of martensitic inelasticity, similar to those caused by the transformational change in temperature [8]. Therefore, it can be argued that the phenomena of martensitic inelasticity are initiated by isothermal mechanocycling.

This article presents the method of experiment and, in part, the results of systematic research on the study of the deformation behaviour of a material with the effect of shape memory, which is in a complex, stress state under conditions of active deformation at constant temperature.

2. MATERIALS AND METHODS

An experimental setup was constructed in the scientific laboratory of Lutsk National Technical University [9], which allows taking readings from the sample separately or simultaneously by stretching or compressing at forces up to 5000 N and torque up to 5 N×m under conditions of change or constant temperature [10].

During the experiment, coaxial fixation was reached by twisting angle of the sample and the axial movement of the end face of the shaft. This allows you to calculate the shear and longitudinal deformation of the sample. Heating was performed using self-propagating high-temperature synthesis [11]. The temperature of the sample during the experiment was recorded using a thermocouple of tungsten rhenium TR5 with a diameter of 100–200 μm [12]. To control the homogeneity of the heating of the sample, two thermocouples used, which were installed at different points.

Method of determining the axial deformation. When determining the axial deformation, the instrumental error associated with the thermal effect of the installation was taken into account [13]. In the installation a reference sample made of St.3 was fixed with a well-known coefficient of thermal linear expansion $\alpha = 1.06\times10^{-5}$ K^{-1} and the dilatogram was determined from the compatible thermal effect of the reference sample and installation [14]. From the obtained total dilatogram, dilatogram of the reference sample was determined, highlighting the thermal effect of this installation. Subsequently, the greenhouse effect of the installation was calculated either by adding it to the reversible composition of the strain during stretching and subtraction during compression. The error in the data of axial deformation was ±0.005 %, and the temperature was ±1 K [15].

The experimental setup made it possible for axial deformation to obtain and fix in isothermal conditions significant inelastic axial deformations during torsion and shear [16].

The samples were made of one batch of saponite–titanium composite rods (Table 1) and had the shape of solid cylindrical rods with a diameter of 5 mm [17]. The length of the working part of the first series was 25 mm, the second – 15 mm, the total length was 55 and 45 mm, respectively. Samples of the second series were used for mechanocycling under conditions of constant or variable compressive force [18].

Table 1. Material for Research

Series of samples	Diameter, mm	Length of a working part, mm	Total length, mm
1	5	25	55
2	5	15	45

The values of the characteristic temperatures of the phase transitions are given in Table 2. Heat treatment of samples was carried out: annealing at a temperature of 820 K for 30 minutes, cooling in the atmosphere.

Table 2. Temperature of Phase Transformations, K

M_1	M_2	A_1	A_2
334	292	382	492

In the first experimental studies (modes I÷III), the samples were twisted with a constant torque with a static voltage τo, and then mechanocycled with an axial voltage. During the second stage (modes IV÷VII), the samples were stretched or compressed, creating a static stress σ, after which they were mechanocycled by torsion [19]. The samples were subjected to isothermal mechanocycling (Fig. 1) at normal or tangential stresses under pulsation cycles under the action of constant orthogonal deformation. The pulsation period or half-period of symmetry of mechanocycles was 120 s.

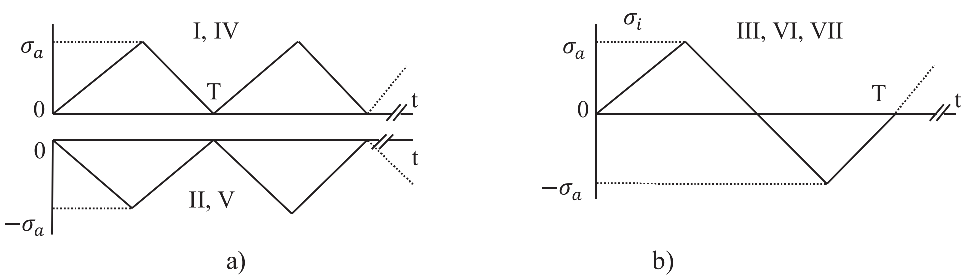

Fig. 1. Load modes: a) static: I and II – torsion, IV – axial tensile deformation, V – compression; b) symmetrical: III – torsion, VI – axial tensile deformation, VII – compression.

Stress intensity due to the static component of the stress state $\sigma_i = \sqrt{3}\,\tau_0$ (where τ_0 is the tangential stress that arises due to the action of static load). The maximum intensity due to the cyclic component of the stress state $\frac{\sigma_i}{\sigma_i^{max}}$ (where σ_a is the amplitude of cyclic stresses) was taken as 50 MPa, 100 MPa, 150 MPa, 200 MPa for both voltages [20].

The intensity of the DC component of the voltage (σ_i) from sample to sample was one of the following: 50 MPa, 100 MPa, 150 MPa, 200 MPa. The amplitude of cyclic stresses $\frac{\sigma_i}{\sigma_i^{max}}$ in a particular sample increased every 12–16 mechanocycles and consistently took all the above values [21].

In this case, in each of the studied samples, the ratio $\frac{\sigma_i}{\sigma_i^{max}}$ in relation to the initial ratio changed equally, successively decreased by 2, 3, 4 times. Experimental studies were performed at three different temperatures (Table 3): martensitic T_M, biphasic T_B and austenitic state T_A of the samples.

Table 3. Temperature for Research, K

T_M	T_B	T_A
320	400	525

The relationship between static loads and amplitudes of cyclic loads are given in Table 4. At each temperature, 16 indicators $K=\frac{\sigma_i}{\sigma_i^{max}}$ were determined. Shear and axial deformations caused by static or alternating cycling stress were recorded [22]. Then one or two mechanocycles were performed without static load in a complex stress state, after which the samples were thermocycled.

Table 4. Load

$K=\frac{\sigma_i}{\sigma_i^{max}}$		σ_i^{max}, MPa			
		50	100	150	200
σ_i, MPa	50	1	0.5	0.33	0.25
	100	2	1	0.67	0.5
	150	3	1.5	1	0.75
	200	4	2	1.33	1

3. EXPERIMENTAL RESULTS AND DISCUSSION

The main results of experimental research are presented in Figs. 2–5. It is shown that the deformation of one component of the deformation always causes a change in the orthogonal component of the deformation, but for different modes and temperatures of deformation the results are different. Some modes are characterised by curves showing the change in the orthogonal component of the deformation from the number of mechanocycles (Figs. 6–8). In the first mechanocycles for all modes of deformation, as a rule, unilateral deformation of the orthogonal component was observed due to static load. In Modes I and II at the martensitic state (Fig. 6a) during axial mechanocycling there was a reverse deformation in the direction of torque (mechanocyclic creep), which practically stopped until the seventh or eighth cycle. The maximum shear deformations were recorded in the conditions of mechanocycling by stretching at amplitudes σ_i^{max} = 200 MPa. Figure 6b shows the dependence of the amount of shear deformation 10 of the cycle on the ratio $\frac{\sigma_i}{\sigma_i^{max}}$. This is due to τ_0 – the magnitude of the static voltage and σ – the amplitude of the pulsating axial voltage. Also, there was a sharp increase in shear deformation with increasing amplitude of normal stress to σ_i^{max} = 200 MPa at a constant $\tau_0 = \frac{100}{\sqrt{3}}$ MPa [23]. The greatest deformation occurred at the usual stress of the opposite sign. Both figures show that tension and compression in a complex stress state have different effects on orthogonal deformation under conditions of mechanocycling in the pulsation mode of the cycle [24].

In Mode III of loading (Fig. 5), the sample shows unusual behaviour where after the third cycle deformation “towards force” stops and passes to the phenomenon of mechanocyclic return, i.e., decreases in the general deformation on an orthogonal component from a cycle to a cycle (curve 6 of Fig. 7) [25]. Thus, this phenomenon can be attributed to negative mechanocyclic creep.

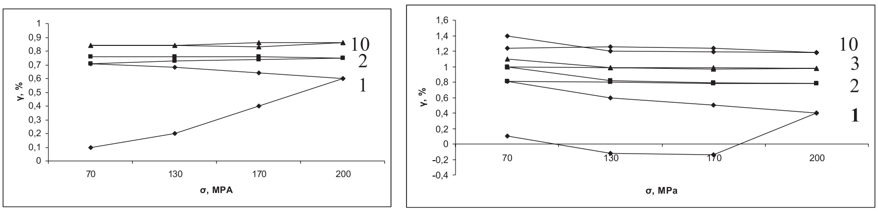

a) b)

Fig. 2. The dependence of shear strain on the normal stress σ in static stress mode I and at $\tau_0 = \frac{50}{\sqrt{3}}$ (a), $\frac{200}{\sqrt{3}}$ MPa (b) and T = 290 K. The figures on the graphs correspond to the numbers of mechanocycles.

In Modes I, II, III, VI, VII after reaching a certain number of cycles (N = 6÷10), an inverse change in deformation was observed (curves 10, Figs. 2, 3a, 4, 5), the value of which in some experiments was 0.35 % for one load cycle (curve 10 in Fig. 2b) [26]. At minimum levels of static stresses, as a rule, deformations were recorded toward a fixed stress at the stage of active deformation and its return during unloading of the sample (curves 10 in Figs. 2 and 3) [27]. With the transition to higher levels of static voltages, the results changed. In this case, the active deformation of one of the components of the stress tensor corresponded to the return of deformation to another and, conversely, the unloading of the sample corresponded to the accumulation of deformation toward a given fixed stress (curve 10 in Figs. 2b, 5). Note that most often reversible deformations were observed in Mode III (curve 15 in Fig. 5). In the process of axial mechanocycling under the conditions of a symmetric cycle, typical properties of martensitic inelasticity appeared, such as shape memory effect under active compression (sections of curves 1 – 1’; 2 – 2’; 3 – 3’, 15 – 15’); plasticity of direct transformation at the subsequent unloading (sections of curves 1’ – 2; 2’ – 3; 3’ – 3”, 15’ – 15”). These phenomena can be considered the effects of martensitic inelasticity, which in this case are initiated by isothermal mechanocycling [28].

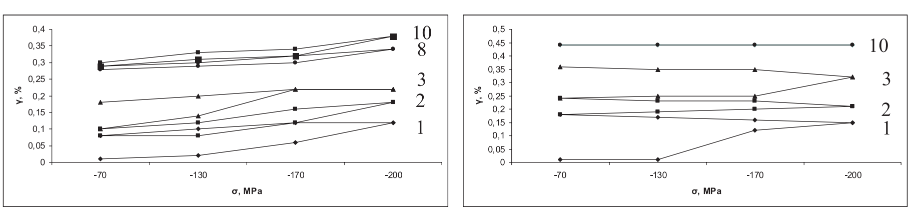

a) b)

Fig. 3. Dependence of shear deformation on the ordinary stress σ in Mode II of static stress and at $\tau_0 = \frac{50}{\sqrt{3}}$ (a), $\frac{200}{\sqrt{3}}$ MPa (b) and T = 290 K.

In the analysis of experimental studies of Mode III for the fifth and tenth mechanocycles with increasing amplitude of the normal stress σ_i^{max}, (σ_i = 50, 100, 150, 200 MPa), change of shear deformation depending on the stress ratio $\frac{\sigma_i}{\sigma_i^{max}}$ and temperatures T has three fundamentally different trends: shear deformation increases with the number of cycles; shear deformation in the process of mechanocycling demonstrates a reverse change; shear deformation gradually decreases with the number of cycles [29].

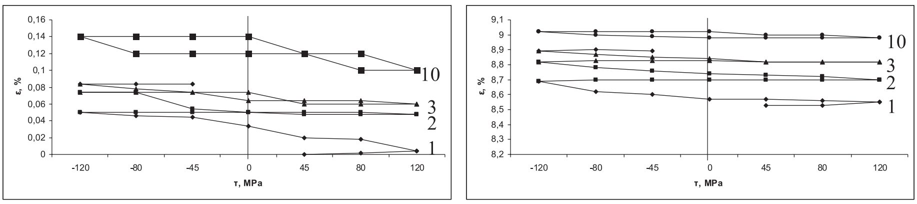

a) b)

Fig. 4. The dependence of the axial deformation on the tangential stress during mechanocycling in Mode VI mode, at the tensile stress σ_i = 50 MPa (a), 200 MPa (b) and T = 290 K.

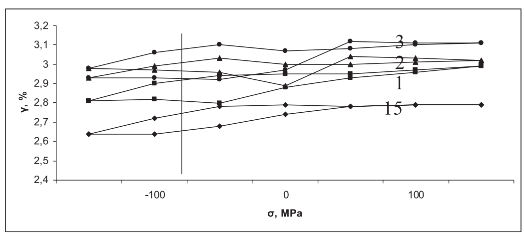

Fig. 5. Dependence of shear shift X axis on σ in Stress Mode III, at τ_0 = 115.5 MPa and T = 290 K.

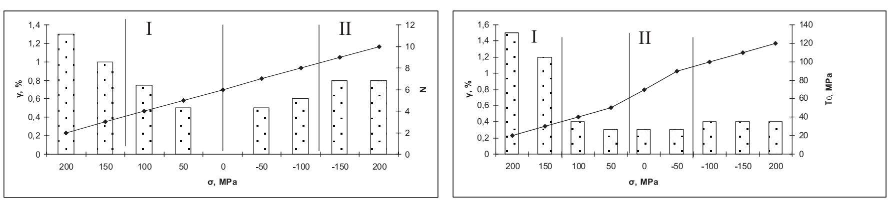

a) b)

Fig. 6. Dependences of shear deformation in Modes I, II at T = 290 K: a) on the number of cycles N and the amplitude of mechanocycling σ at $\tau_0 = \frac{200}{\sqrt{3}}$ MPa; b) the magnitude of static voltage and the amplitude of mechanocycling σ γ.

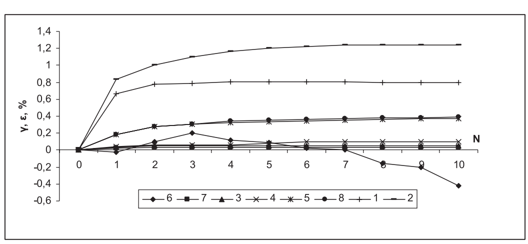

Fig. 7. Dependences of shear (1÷6) and axial (7÷8) deformations formed in the process of mechanocycling on the number of cycles for Modes: I (1, 2) at (1, 2) at σ_i = 50 MPa and σ_a = 200 MPa (1), σ_i = 200 MPa and σ_a = 200 MPa (2); II (3 ÷ 5) at σ_i = 50 MPa and σ_a = 100 MPa (3), σ_a = 200 MPa (4), σ_i = 200 MPa and σ_a = 200 MPa (5); III (6) at σ_i = 50 MPa and σ_a = 150 MPa (6); VI (7, 8) at σ_i = 200 MPa and σ_a = 50 MPa (7), σ_a = 200 MPa (8) at T = 290 K.

Figure 8 presents the dependence of orthogonal shear deformation on the number of cycles with additional and negative axial deformation in Mode III mode under conditions of gradual change of amplitude of normal stress for different relations $K = \frac{\sigma_i}{\sigma_i^{max}}$ between static stress and amplitude of cyclic stress change [30].

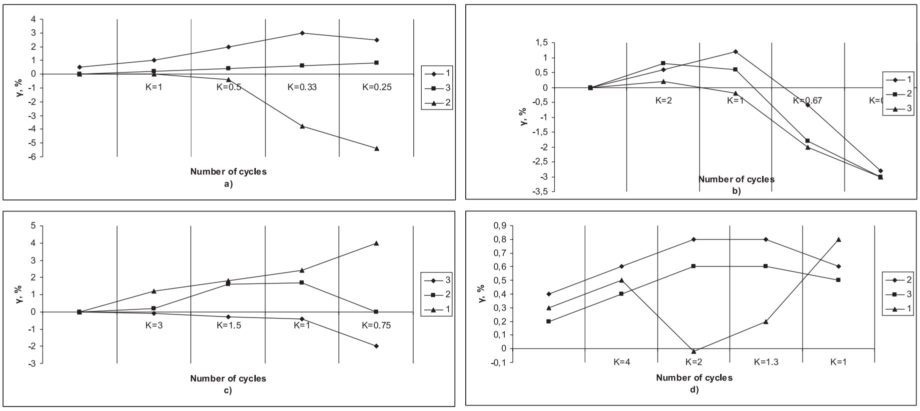

Fig. 8. Dependence of shear deformation on the number with additional and negative axial deformation (Mode III) under conditions of gradual change of amplitude of normal stress σ_a = 50 (region I), 100 (II), 150 (III), 200 MPa IV) at T = 290 K (1), 370 K (2), 510 K (3), for the values σ_i = 50 (a), 100 (b), 150 (c), 200 MPa (d).

At the lowest σ_i = 50 MPa (Fig. 8), the value of the mechanocyclic return reaches the maximum value at a temperature corresponding to the two-phase state (curve 2a). At σ_i = 100 MPa (Fig. 8b), there is the same, almost synchronous, increase, and then the shear deformation decreases at all temperatures, i.e., the sample with increasing amplitude of the axial stress of “untwisting”. For σ_i = 150 MPa (Fig. 8c) in the martensitic state (curve 1c) with increasing number of mechanocycles shear deformation accumulated in the direction of constant tangential stress increases. At a temperature of 370 K after some increase in deformation, there is a negative mechanocyclic creep. It leads to the initial level of shear deformation at higher values of σ_i^{max} = 200 MPa. At a temperature corresponding to the austenitic state of the sample, a gradual mechanocyclic return is observed. For all temperatures at σ_i = 200 MPa (Fig. 8d), slight changes in shear deformation are observed [31].

Therefore, according to the results of experimental data, in the martensitic state it is impossible to unambiguously determine the change in the deformation shift (its increase or decrease) in the process of mechanocycling along the axial stress component, i.e., there is no necessary dependence on the parameter $K = \frac{\sigma_i}{\sigma_i^{max}}$. In the two-phase state, the orthogonal component of the deformation increases only when K > 1, i.e., the sample “twists” in the direction of static torque; in the case of K ≤ 1 the sample begins to “untwist”. In the austenitic state, it is impossible to unambiguously link the change in shear deformation with the parameter K; however, it can be noted that it practically does not change at the minimum and maximum values of σ_i, namely, at 50 and 200 MPa [32].

Analysing all experimental data on isothermal mechanocycling of continuous cylindrical samples of saponite–titanium composites in Mode III in the martensitic state, in 56 % of cases of different ratios $K = \frac{\sigma_i}{\sigma_i^{max}}$ there is only an increase in shear deformation, i.e., an increase towards constant torque. Mechanocyclic return is mainly observed after 5–7 cycles, and provided that the intensity of the static and dynamic components of the loads at K = 1. It is observed that in the two-phase state at K > 1 there is only accumulation of deformation, and at K ≤ 1 only return of deformation (during the first stage of 5–7 cycles, in the second and subsequent with the first mechanocycle). In the austenitic state, either accumulation of deformation (54 % of cases) or return from the first mechanocycle was detected. At the amplitude of cyclic stresses σ_a = 50 MPa at all temperatures in 85 % of all experiments there is an accumulation of shear component deformation.

4. CONCLUSIONS

In the study of isothermal cycling of saponite–titanium composites under conditions of complex stress state, the martensitic stress has a number of factors. The first is mechanocyclic creep, which usually leads to irreversible accumulated deformation towards a fixed stress. This may be due to the texturing of the material in the process of mechanical cycling, as well as the evolution of oriented and undirected internal microvoltages. As the cycles are repeated, there is a mechanical slander, which significantly reduces the intensity of deformation accumulation and leads to its saturation. The second factor is along with the irreversible deformation of mechanocycling. According to the Clausius-Clapeyron ratio, it can be accompanied by direct and inverse martensitic reactions and lead to reversible deformation of the material. This also applies to Modes IV and V, as well as some schemes of Loaded Mode II. Of greatest interest is the case when, along with the reversible deformation in the process of mechanocycling, there is a mechanocyclic return of the orthogonal component of the deformation or a negative mechanocyclic creep. This phenomenon is obviously due to the fact that at the initial stage of the mechanocycle there is an accumulation of irreversible deformation, which is realised more due to the channels of martensitic inelasticity. After a certain number of cycles, irreversible complex deformations occur. It is almost completely neutralized due to mechanical hardening, as a result of which the restoration of deformation from cycle to cycle begins to appear.

Analysing the results of research, we can draw the following conclusions:

The mechanocycle on one component of deformation always causes change of orthogonal deformations. In the first cycles, in all load modes, there is a gradual accumulation towards the load.

With the accumulation of a certain number of cycles there is an inverse deformation or complete independence of the deformation from the number of cycles.

The strongest effect of reversible deformation is manifested in Mode III, if the cycling is carried out in a symmetrical cycle "stretching – unloading – compression – unloading".

Mode III is characterised by the phenomenon of return mechanocycling, which has the largest value at small values of τ_0 = 50 MPa at a temperature corresponding to the two-phase state.

Different influence on the shear of half-compression and tensile deformation is recorded. In the two-phase state with increasing number of cycles the semi-cycle of compression has a predominant effect on shear deformation and in this state at $\frac{\sigma_i}{\sigma_i^{max}} = 1$ there is a clear change of sign with increasing shear deformation. In the austenitic state, the semi-cycle of stretching has the predominant effect. In the martensitic state during semi-stretching and compression, changes do not occur.

Therefore, some of these phenomena can be explained by the presence of martensitic reactions that occur during mechanocycling [3].

REFERENCES

1. Yuan, H., Fauroux, J.–Ch., Chapelle, F., & Balandraud, X. (2017). A Review of Rotary Actuators Based on Shape Memory Alloys. *Journal of Intelligent Material Systems and Structures, 28* (14), 1863–1885, DOI: org/10.1177/1045389X16682848
2. Lavakumar, A. (2017). Mechanical Properties of Materials. *Concepts in Physical Metallurgy, 4,* 5–22. https://doi.org/10.1088/978-1-6817-4473-5ch5
3. Huliieva, N. M., Somov, D. O., Pasternak, V. V., Samchuk L. M., & Chetverzhuk, T. I. (2020). The Selection of Boron Nitride Circles for Grinding Saponite – Titanium Composites Using Non-Parametric Method. *Latvian Journal of Physics and Technical Sciences, 57* (6), 68–77. DOI: 10.2478/lpts-2020-0033
4. Tahara, M., Kim, H. Yo., Hosoda, H., & Miyazaki, Sh. (2009). Shape Memory Effect and Cyclic Deformation Behavior of Ti–Nb–N Alloys. *Functional Materials Letters, 2* (2), 79–82. DOI: org/10.1142/S1793604709000600
5. Sun, Q., Cao, B., Iwamoto, T., & Suo, T. (2021). Effect of Impact Deformation on Shape Recovery Behavior in Fe-Mn-Si Shape Memory Alloy under Shape Memory Training Process with Cyclic Thermo-Mechanical Loading. *Science China Technological Sciences*. DOI: org/10.1007/s11431-020-1759-y
6. Zabolotnyi, O., Pasternak, V., Ilchuk, N., Huliieva, N., & Cagáňová, D. (2021). Powder technology and software tools for microstructure control of $AlCu_2$ samples. In: *Proceedings of the 4th Int. Conf. on Design, Simulation and Manufacturing: The Innovation Exchange, DSMIE-2021* (pp. 585–593), 8–11 June 2021. Lviv, Ukraine: Manufacturing and Materials Engineering: Springer.
7. Ohki, T., Ni, Q.-Q., Ohsako, N., & Iwamoto, M. (2004). Mechanical and Shape Memory Behavior of Composites with Shape Memory Polymer. *Composites Part A: Applied Science and Manufacturing*, *35* (9), 1065–1073. DOI:org/10.1016/j.compositesa.2004.03.001
8. Murasawa, G., Tohgo, K., & Ishii, H. (2004). Deformation Behavior of NiTi / Polymer Shape Memory Alloy Composites – Experimental Verifications. *Journal of Composite Materials, 38* (5), 399–416. DOI: org/10.1177/0021998304040553
9. Turov, V., Tryasuchev, L., Klochko, V., & Zvonytsky V. (2008). IPC Tensile Testing Device. N 33345. *Database of Patents of Ukraine.* Available at https://uapatents.com/3-33345-pristrijj-dlya-viprobuvannya-na-roztyag-stisk.html
10. Sheldon, B.W., Rajamani, A., Bhandari, A., Chason, E., Hong, S.K., & Beresford, R. (2005). Competition between Tensile and Compressive Stress Mechanisms during Volmer-Weber Growth of Aluminum Nitride Films. *Journal of Applied Physics, 98,* 043509. DOI:org/10.1063/1.1994944
11. Patent of Ukraine 91287, IPC B22F 3/23 (2006.01) C01G 1/00 (2014.01). Reactor for Self-propagating High-Temperature Synthesis (SHS process). L. Samchuk, N. Guliyeva, V. Rud, O. Povstyanoy, I. Savyuk, Yu. Vorobey, M. Zaikin. Lutsk National Technical University, Lutsk, 25.06.14, 12.
12. Rud, V., Samchuk, L., & Guliieva, N. (2014). Application of Pyrometric Technique for Imaging of Front SHS Burning. *Bulletin of Vinnytsia Polytechnic Institute: Mechanical Engineering and Transport. Vinnitsa, 6,* 97–101.
13. Shmyg, R., Boyarchuk, V., Dobryansky, I., Barabash V., & Schmig, R.A. (2010). Measurement Error. *Terminological Dictionary-Reference Book on Construction and Architecture*. Lviv, 159.

14. Standard. (2017). *ISO 12106:2017*. Metallic Materials. Fatigue Testing. Axial-Strain-Controlled Method, 38.
15. Anwar, N., & Najam, F. (2017). Chapter Three – Axial-Flexual Response of Cross-Sections. *Structural Cross Sections Analysis and Design*, 137–249.
16. Huliieva, N. (2019). Exposure to Saponite-Titanium Composite with Subsequent Deformation of Intense Plastic Torsional Deformation. *Abstracts of the VI Scientific Conference Nanoscale Systems: Structure, Properties, Technologies* (pp. 3–6), Kyiv: NANSIS 2019.
17. Huliieva, N., Pasternak, V., & Samchuk, L. (2020). Application of deep sanding method of saponite – titanium blanks. In: *VI International Scientific and Practical Conference Scientific Achievements of Modern Society* (p. 119), 5–7 February 2020. Liverpool: UK.
18. Sheremetyev, V., Prokoshkin, S., Brailovski, V., & Dubinskiy, S. (2015). Investigation of the Structure Stability and Superelastic Behavior of Thermomechanically Treated Ti-Nb-Zr and Ti-Nb-Ta Shape-Memory Alloys. *The Physics of Metals and Metallography, 116* (4), 413–422. DOI: 10.1134/S0031918X15040158
19. Ropyak, L., & Velichkovych, A. (2016). *Investigation of the Stress State of a Multifunctional Coating during Stretching or Torsion.* Kyiv: KPI them. Igor Sikorsky, 194–196.
20. Gomatam, R., & Sancaktar, E. (2006). The Effects of Stress State, Loading Frequency and Cyclic Waveforms on the Fatigue Behavior of Silver-Filled Electronically-Conductive Adhesive Joints. *January Journal of Adhesion Science and Technology, 20* (1), 53–68. DOI: 10.1163/156856106775212378.
21. Ma, Z., Zhao, H., & Liu, Ch. (2021). Prediction Method of Low Cyclic Stress-Strain Curve of Structural Materials. *Materials Transactions, 56* (7), 1067–1071. DOI: 10.2320/matertrans. M2015085]
22. Gooch, Ja. (2011). Cyclic Stress Strain. *Encyclopedic Dictionary of Polymers*, 189–189. DOI: 10.1007/978-1-4419-6247-8_3235
23. Kelly, Ja. (2017). Shear Deformation and the Buckling of Columns, Revisited. *Civil Eng Res J. 2* (1), 555579. DOI:10.19080/CERJ.2017.02.555579
24. Herrmann, H., & Bucksch, H. (1991). Shear deformation. *Dictionary Geotechnical Engineering/Wörterbuch GeoTechnik,* 2633–3379. Springer, Berlin, Heidelberg. DOI: 10.1007/978-3-642-41714-6_192792
25. Bhaskar, K., & Varadan, T. (2021). Shear Deformation Theories (pp. 181–195). In: *Plates*. Springer, Cham. DOI: org/10.1007/978-3-030-69424-1_11
26. Casati, R., Vedani, M., & Tuissi A. (2014). Thermal Cycling of Stress-Induced Martensite for High-Performance Shape Memory Effect. *Scripta Materialia*, *80*, 13–16. DOI:10.1016/j.scriptamat.2014.02.003
27. Lázpita, P., Villa, E., Villa, F., & Chernenko, V. (2021). Temperature Dependent Stress–Strain Behavior and Martensite Stabilization in Magnetic Shape Memory $Ni_{51.1}Fe_{16.4}Ga_{26.3}Co_{6.2}$. *Single Crystal Metals*, *11*, 920. DOI: org/10.3390/met11060920
28. Müllner, P., Chernenko, V., & Kostorz, G. (2004). Large Cyclic Magnetic-Field-Induced Deformation in Orthorhombic (14M) Ni–Mn–Ga Martensite. *J. Appl. Phys, 95*, 1531–1536.
29. Pagounis, E., & Muellner, P. (2018). Materials and actuator solutions for advanced magnetic shape memory devices. In: Proceedings of the ACTUATOR 2018, 16th International Conference on New Actuators (pp. 1–7), 25–27 June 2018. Bremen, Germany.
30. Kustov, S., Pons, J., Cesari, E., & Van Humbeeck, J. (2004). Chemical and Mechanical Stabilization of Martensite. *Acta Mater, 52*, 4547–4559.
31. Samy, N., Daróczi, L., Tóth, L., Panchenko, E., Chumlyakov, Y., Surikov, N., & Beke, D. (2020). Effect of Stress-Induced Martensite Stabilization on Acoustic Emission Characteristics and the Entropy of Martensitic Transformation in Shape Memory $Ni_{51}Fe_{18}Ga_{27}Co_{4}$ Single Crystal. *Metals*, *10*, 534.
32. Roytburd, A. (2000). Intrinsic Hysteresis of Superelastic Deformation. *Mater. Sci. Forum*, 389–392.